

DOI: 10.1002/cphc.201200974

# Autoionization of Molecular Hydrogen: Where do the Fano Lineshapes Go?

Alicia Palacios,<sup>\*[a]</sup> Johannes Feist,<sup>[b]</sup> Alberto González-Castrillo,<sup>[a]</sup> José Luis Sanz-Vicario,<sup>[c]</sup> and Fernando Martín<sup>[a, d]</sup>

Atomic autoionization following photoabsorption is a typical example of quantum interferences governed by electron–electron correlation. Coherence between direct photoionization and autoionization paths results in “Fano profiles”, widely explored in atoms in the last 60 years. The advent of femto- and attosecond laser technology made time-resolved images of the delayed electron ejection in autoionization accessible, leading to the reemergence of such studies in atomic systems. The counterpart molecular phenomena show the richness, as well as the complexity, added by nuclear motion, which may proceed on similar time scales. However, Fano profiles are usually absent in measured molecular photoionization cross sections and an unequivocal parametrization of molecular autoioniza-

tion signatures, similar to that introduced by Fano in atoms [U. Fano, *Phys. Rev.* **1961**, *124*, 1866] has not yet been achieved. In this work we introduce a simple semiclassical model that accounts for all the features observed in H<sub>2</sub> photoionization and demonstrate that the interference structures observed in dissociative ionization spectra are almost exclusively due to the phase accumulated in the nuclear motion. Furthermore, we show that the temporal build-up of these structures in the energy-differential cross sections is also determined by nuclear motion. We validate our models by comparing with full-dimensional ab initio calculations solving the time-dependent Schrödinger equation.

## 1. Introduction

Our knowledge of gas-phase molecular dynamics, which enables the understanding of a wide range of fundamental chemical processes,<sup>[1–4]</sup> has rapidly been growing since the development of ultrashort pulse sources. The availability of pulses in the femtosecond (fs) and attosecond (as) regimes<sup>[5–8]</sup> together with the most advanced detection techniques<sup>[2,9,10]</sup> give access to real-time images of field-generated nuclear dynamics.<sup>[4]</sup> Recent experiments have managed to trace the much faster electron motion, tracking the temporal evolution of bound or quasibound coherently excited electron wave packets in atoms.<sup>[11,12]</sup> In particular, measurements that make use of isolated attosecond pulses in the extreme ultraviolet regime<sup>[6,8,13]</sup>

have demonstrated the suitability of these novel radiation sources to explore fundamental processes in atomic physics governed by electron–electron interactions such as Auger decay<sup>[14]</sup> or atomic autoionization<sup>[15]</sup> on their intrinsic time scales.

The state-of-the-art in laser technology is thus ready to explore, with unprecedented time and space resolution, processes where electron correlation may play an important role. Studies on decay processes are particularly interesting given that the absence of the field reveals the intrinsic characteristics of matter. In this framework, autoionization of atomic targets through the decay of doubly excited states (DES) is an ideal candidate. The well-known “Fano lineshape”, found in atomic photoionization cross sections as a result of the quantum interference between autoionization and direct photoionization paths, was already described around 50 years ago.<sup>[16]</sup> Formation of Fano resonances is an archetype dynamical process of quantum coherence in non-stationary systems. Nevertheless, time-resolved images of this process have only very recently become the focus of theoretical investigations.<sup>[17–20]</sup> These latter works show the build-up of the Fano profile in time, which can be recorded by means of different techniques such as by using moderately intense mid-IR lasers,<sup>[20]</sup> or attosecond streaking techniques,<sup>[17]</sup> or a near-IR fs laser such as that employed in ref. [15] to resolve the autoionization decay of the 2s2p(<sup>1</sup>P<sup>o</sup>) doubly excited state of He in time.


The counterpart time-resolved studies on molecules are scarcer due to the complexity added by the nuclear motion, which takes place while the electron is being ejected from the

[a] Dr. A. Palacios, A. González-Castrillo, Prof. F. Martín  
Departamento de Química, Modulo 13  
Universidad Autónoma de Madrid  
28049 Madrid (Spain)  
E-mail: alicia.palacios@uam.es

[b] Dr. J. Feist  
ITAMP  
Harvard-Smithsonian Center for Astrophysics  
Cambridge, Massachusetts 02138 (USA)

[c] Prof. J. L. Sanz-Vicario  
Grupo de Física Atómica y Molecular  
Instituto de Física, Universidad de Antioquia  
Medellín (Colombia)

[d] Prof. F. Martín  
Instituto Madrileño de Estudios Avanzados en Nanociencia  
Cantoblanco, 28049 Madrid (Spain)

 Supporting information for this article is available on the WWW under <http://dx.doi.org/10.1002/cphc.201200974>.

autoionizing states. In this context, molecular descriptions of autoionization based on the fixed-nuclei approximation are a priori out of the question. Although an accurate theoretical method incorporating both electronic and nuclear degrees of freedom in a quantum manner and in the time domain already exists<sup>[21–24]</sup> and has successfully been applied to study H<sub>2</sub> autoionization,<sup>[23,25–31]</sup> and although as-UV pump/fs-IR probe experiments in this molecule<sup>[28]</sup> have already been able to detect the contribution of DES through the analysis of laboratory-frame proton ejection asymmetries, a simple time-resolved picture of molecular autoionization similar to that existing for atoms has not yet been achieved. For example, Fano lineshapes are a clear signature of autoionization in atoms, but no analogue is known for molecules, although it is reasonable to ask if a similar expression would apply. A related question is: do the nuclei introduce decoherence in the Fano interference structures?<sup>[32]</sup>

The present work addresses this key point, focusing on the dissociative ionization process, which leads to the clearest signature of autoionization in H<sub>2</sub> and D<sub>2</sub>.<sup>[33–35]</sup> This work consists of two parts. In section 2, we present a simple model, not previously proposed in the literature to our knowledge, to explain the features arising in the kinetic energy distributions of electrons and nuclei in the autoionization region. In section 3, we explore the build-up of these features in time by including classical motion in the model and comparing it with ab initio calculations that solve the time-dependent Schrödinger equation.

## 2. Molecular Autoionization Model

Since the first evidence of doubly excited states (DESs) in H<sub>2</sub>, obtained in 1967,<sup>[36]</sup> several experimental groups have explored photoionization of both H<sub>2</sub> and D<sub>2</sub> in the energy region where the first two series of DESs are manifest, such as the synchrotron radiation experiments of Latimer et al.<sup>[33,34,37]</sup> and Ito et al.<sup>[35]</sup> (see ref. [38] for a review). Recent works have even measured accurate energy and angular differential photoionization cross sections,<sup>[39,40]</sup> thus enabling the study of interferences arising from different DESs populated by synchrotron radiation<sup>[41]</sup> or laser pulses generated by high-order harmonics.<sup>[42]</sup> The present section of the manuscript is devoted to find the simplest model that describes energy-differential photoionization in the region of the autoionizing states. The results of the model will be compared with accurate ab initio calculations whose excellent agreement with the experiments by Ito et al.<sup>[35]</sup> has been previously shown.<sup>[38]</sup>

As mentioned above, we focus on the dissociative photoionization process, H<sub>2</sub> +  $\gamma$  → H + H<sup>+</sup> + e<sup>-</sup>, and include only one doubly excited state in our model, the lowest Q<sub>1</sub> <sup>1</sup>Σ<sub>u</sub><sup>+</sup> state. Figure 1 shows the relevant potential energy curves. For small and intermediate values of the internuclear distance *R*, the potential energy curve of the DES [*V*<sub>Q</sub>(*R*)] is embedded in the single ionization continuum associated with the H<sub>2</sub><sup>+</sup> 1s σ<sub>g</sub> ground state, whose potential energy curve is given by *V*<sub>P</sub>(*R*). The coupling with the continuum, mediated by the electron–

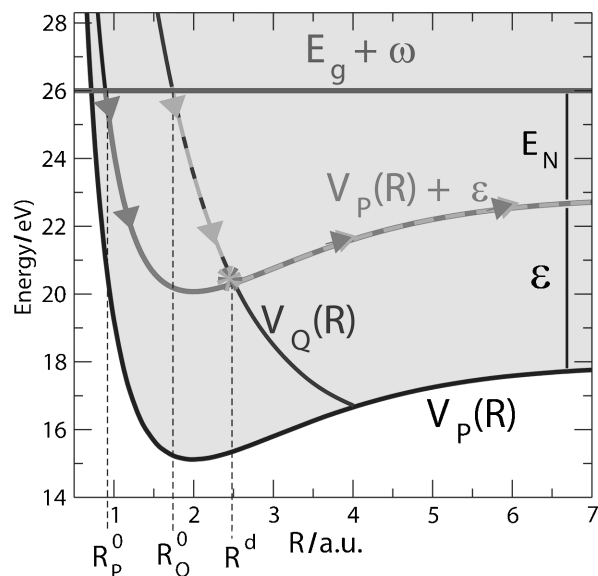


**Figure 1.** Potential energy curves of the H<sub>2</sub><sup>+</sup> ground state [*V*<sub>P</sub>(*R*)] and lowest H<sub>2</sub> DES of <sup>1</sup>Σ<sub>u</sub><sup>+</sup> symmetry in the Q<sub>1</sub> series [*V*<sub>Q</sub>(*R*)]. Also indicated are the semi-classical nuclear paths included in our model, for both the DES and the electronic continuum associated with *V*<sub>P</sub>, where  $\epsilon$  represents the energy of the ejected electron. The total energy  $E_g + \omega$  reached after photoabsorption from the lowest vibronic state in the ground state *g* (not included in the figure) is distributed among the photofragments (nuclei with energy  $E_N$  and the electron with energy  $\epsilon$ ) such that  $\epsilon + E_N + V_P(R \rightarrow \infty) = E_g + \omega$ .  $R_p^0$  and  $R_Q^0$  denote the classical turning points for the  $V_P + \epsilon$  and  $V_Q$  curves, respectively, for the given total energy, and  $R^d$  indicates the internuclear distance at which the DES eventually decays into a continuum state with energy  $V_P(R) + \epsilon$ . The energy scale starts at  $E_g = 0$ , and the *y*-axis thus directly indicates the photon energy (in eV).

electron interaction, transforms the bound state into a quasi-bound resonance with decay rate  $\Gamma(R)$ .

For photoionization, as in atoms, there are two interfering paths leading to the same final state: direct ionization to the continuum and resonant excitation to the DES followed by autoionizing decay into the continuum. For infinitely heavy nuclei (i.e. in the fixed-nuclei approximation), the molecule behaves exactly like an atom and, consequently, Fano profiles are found.<sup>[43]</sup> However, the extra nuclear degree(s) of freedom modify this behavior significantly: First, the DES can be resonantly excited over a wide range of photon energies because of the *R*-dependence of the energy levels within the Franck–Condon region, which already implies an averaging effect. Second, nuclear motion proceeds on similar timescales as autoionization, making the phase accumulated in nuclear propagation relevant. The combination of these two effects renders the disappearance of Fano profiles plausible. However, since the dynamics is fully coherent, quantum interference between the direct and autoionizing paths should still occur, albeit in a different manifestation.

We explore the problem in more detail by using both semi-classical and quantum mechanical approaches, following the footsteps of Miller<sup>[44]</sup> and his work on Penning ionization. He formally described the process  $A^* + B \rightarrow A + B^+ + e^-$ , where initially the atom *A* is in an excited electronic state and the atom *B* is in its ground state. Roughly speaking, photoionization can

be seen as the half-collision problem related to Penning autoionization but with a non-zero background continuum amplitude. In the particular case of hydrogenic molecules, direct photoionization is the largest contribution (> 95%) and its dissociative contribution mainly ejects protons with low kinetic energies. It is thus in this energy region where interference is largely visible. In refs. [33, 34, 37] Latimer and collaborators also attempted to extract the autoionization widths as a function of the internuclear distance,  $\Gamma(R)$ , by using a semiclassical expression for the decay probability [Eq. (1)].<sup>[44–46]</sup>

$$P(R) = \frac{\Gamma(R)}{\hbar\nu(R)} \exp\left(-\int_{R_0}^R \frac{\Gamma(R')}{\hbar\nu(R')} dR'\right) \quad (1)$$

where  $\Gamma(R)$  is the molecular decay width and  $\nu(R)$  is the radial velocity of the nuclei. However, Equation (1) only accounts for autoionization, missing the coherent addition of the direct photoionization contribution. It is therefore only meaningful in the absence of the direct path. This is the case for DES in the  $Q_2$  and higher series for some target symmetries ( $^1\Pi_u$ ).<sup>[47]</sup> An accurate description, including the interferences mentioned above, energy positions and autoionization widths for different symmetries and series of DES was only accomplished in the late nineties, with the first full-dimensional ab initio calculations on hydrogenic molecules.<sup>[38, 47–49]</sup> These accurate calculations allowed the unequivocal assignment of the signature resulting from the strong coupling between the resonant and non-resonant continua contributions in the nuclear kinetic energy distributions (KEDs). Nevertheless, and regardless of the accuracy of the theoretical approach employed in refs. [47–49], a simple expression accounting for the interferences shown in the KEDs is still missing. In the following, we propose a manageable semiclassical model that, besides the description of such features, allows for a simpler understanding of the relevant electronic and nuclear dependencies of the autoionization signatures in molecules.

We briefly review the situation for atoms (or, equivalently, molecules in the fixed nuclei approximation), following Fano.<sup>[16]</sup> For brevity, we take the relevant matrix elements to be independent of energy in the following. The transition amplitude from the initial state  $\psi_0$  to a continuum state  $\psi_\varepsilon$  can then be written as Equation (2):

$$\langle \psi_\varepsilon | T | \psi_0 \rangle = c_Q \sin \Delta - c_P \cos \Delta \quad (2)$$

where  $\varepsilon$  is the energy of the emitted electron,  $c_Q$  is related to the transition matrix element to the quasi-bound state and  $c_P$  is the matrix element to the background continuum (the labels  $P$  and  $Q$  follow Feshbach notation),<sup>[50]</sup> while  $\Delta = -\arctan \frac{\Gamma/2}{\varepsilon - E_r}$ , with  $E_r$  and  $\Gamma$  the resonance position and width, respectively. The cross section ( $\propto |\langle \psi_\varepsilon | T | \psi_0 \rangle|^2$ ) then shows a well-known asymmetric Fano profile, where the two contributions interfere destructively on one side of the resonance and constructively on the other. Conceptually, the observed profile is a consequence of a flat background contribution interfering with a resonant contribution of width  $\Gamma$ , the phase of which goes through a  $\pi$  phase jump as the resonance is crossed.

As we show in the following, the situation is both simpler and more complex in molecules. As the resonance energy depends on  $R$ , the photon can hit the center of the resonance for a broad range of energies, and this part dominates the resonant contribution. Consequently, there is no phase jump as the resonance is crossed, except possibly at the extremes of the Franck–Condon region. However, the complicating factor is nuclear motion, which adds an additional phase. As a second consequence, the dominant contributions from the direct and autoionizing path for a given final electronic and nuclear kinetic energy are not expected to originate from the same initial  $R$ .

In our model, we consider that for a given photon energy,  $\omega$ , the ionization amplitude as a function of the ejected electron energy,  $\varepsilon$ , can be written as the sum of a direct photoionization amplitude  $c_p$  from the ground state and an amplitude  $a_Q$  for the resonant component. Therefore the dissociative ionization probability, accounting for autoionization from an isolated DES, can be written as Equation (3):

$$P(\varepsilon, \omega) = |c_p e^{-i\theta_p} e^{-i\delta_\varepsilon} + a_Q e^{-i\theta_Q}|^2 \quad (3)$$

where the arbitrary phase  $\delta_\varepsilon$  is introduced to account for the phase difference in the dipole electronic transitions, and  $\theta_p$  and  $\theta_Q$  in Equation (3) are the accumulated phases of the nuclei moving on a given potential energy curve ( $V_p$  and  $V_Q$  respectively), which we estimate with the WKB approximation [Eqs. (4a) and (4b)]:

$$\theta_p = \int_{R_p^0}^{R^d} dR \sqrt{2 \cdot \mu [\omega - V_p(R) - \varepsilon]} \quad (4a)$$

$$\theta_Q = \int_{R_Q^0}^{R^d} dR \sqrt{2 \cdot \mu [\omega - V_Q(R)]} \quad (4b)$$

This assumes that only a single classical path contributes for each of the two amplitudes. These classical paths are pictured in Figure 1 for one-photon absorption from the vibronic ground state with energy  $E_g$ . The total excess energy  $E_T$  available after overcoming the dissociation limit ( $D = V_p(R \rightarrow \infty) - E_g \approx 18.15$  eV) is to be shared between electrons and nuclei:  $E_T = \omega - D = \varepsilon + E_N$ . The lower limits of the integrals in Equations (4) depend only on photon energy ( $R_p^0$ ) and on both photon and electron energy ( $R_Q^0$ ), respectively. They correspond to the internuclear distances at which the electronic energies  $V_Q(R)$  and  $V_p(R) + \varepsilon$  are equal to  $E_g + \omega$ , as follows from the reflection approximation (see Supporting Information). In a more complete model, the contributions from all  $R_Q^0$  for which  $E_T$  is within the decay width should be coherently added. The current model neglects this, as well as the variation of the phase shift  $\Delta$  across the resonance that is responsible for the appearance of Fano profiles in atoms. This phase shift is simply replaced by the energy-independent quantity  $\delta_\varepsilon$ .

The integrals in Equation (4) in principle extend to  $R = \infty$ , however after the decay of the DES both paths proceed on the same ionic potential curve and accumulate an identical phase. The upper limit ( $R^d$ ) is thus fixed at the  $R$  value at which decay takes place, that is, where the DES will eject an electron

of energy  $\varepsilon$ , given by  $V_p(R^d) + \varepsilon = V_Q(R^d)$ . Note that the value of  $R^d$  depends only on  $\varepsilon$ .

For dissociative ionization, the direct path leads to an exponentially decaying distribution as a function of nuclear kinetic energy that is independent of photon energy and simply follows the Franck-Condon (FC) overlap from the ground state. On the other hand, the autoionization amplitude ( $a_Q$ ) can be written in semiclassical mechanics as a product of a term ( $c_Q$ ) accounting for the transition from the ground state to the quasi-bound DES, and a term describing the decay into the non-resonant background defined in Equation (1), leading to Equation (5):<sup>[44]</sup>

$$a_Q = \sqrt{\frac{1}{|V'_Q(R^d) - V'_p(R^d)|}} \sqrt{\frac{\Gamma(R^d)}{\hbar v_Q(R^d)}} c_Q e^{-\theta_{Qr}} \quad (5)$$

where the prefactor with the square root of the derivatives comes from rewriting the probability as a function of energy ( $P(\varepsilon)d\varepsilon = P(R)dR$ ) and  $\theta_{Qr}$  is one half of the integral in Equation (1), which is consistently integrated from  $R_Q^0$  to  $R^d$ .

The amplitudes  $c_p$  and  $c_Q$  then correspond to the actual components of the dipole transition elements from the vibronic ground state to the vibronic continua ( $P$ ) and DES, respectively. In a further simplification, we can now use the Franck-Condon (FC) approximation in separating the electronic and nuclear components of the total wave function [ $\Psi(\mathbf{r}, R) = \psi(\mathbf{r}, R)\chi(R)$ ] and neglecting the dependence of the electronic matrix elements on the nuclear position. This leads to writing the amplitudes as Equation (6):

$$\begin{aligned} c_p(\varepsilon, \omega) &= \langle \chi_p(R) | \chi_{g_0}(R) \rangle d_p \\ c_Q(\omega) &= \langle \chi_Q(R) | \chi_{g_0}(R) \rangle d_Q \end{aligned} \quad (6)$$

where the actual dipole couplings among electronic wave functions are approximated to be independent of  $R$  [Eq. (7)]:

$$\begin{aligned} d_p &= \langle \psi_p(\mathbf{r}, R_e) | \hat{D} | \psi_0(\mathbf{r}, R_e) \rangle \\ d_Q &= \langle \psi_Q(\mathbf{r}, R_e) | \hat{D} | \psi_0(\mathbf{r}, R_e) \rangle \end{aligned} \quad (7)$$

with  $\hat{D}$  the dipole operator,  $\psi_0$  the initial electronic state,  $\psi_p$  the nonresonant continuum state,  $\psi_Q$  the DES, and  $R_e$  the equilibrium internuclear distance.

At this point Equation (3) can be evaluated using as inputs the calculated vibronic ground state, the potential curves  $V_Q(R)$  and  $V_p(R)$ , and the  $\Gamma(R)$  function; only leaving free the values of  $\delta_c$ ,  $d_Q$  and  $d_p$  in a fit to the cross sections. For the vibrational overlaps in Equation (6) we use the straightforward reflection approximation (see Supporting Information). The results of this first approach are plotted as dashed lines in Figure 2 for the dissociative photoionization of  $H_2$  (left panels) and  $D_2$  (right panels) as a function of the proton/deuteron kinetic energy. Note that according to the previous notation PKE and DKE are equal to  $E_N/2$ . We compare with the accurate time-independent calculations published in ref. [48] for photoionization at four different photon energies using linearly polarized light

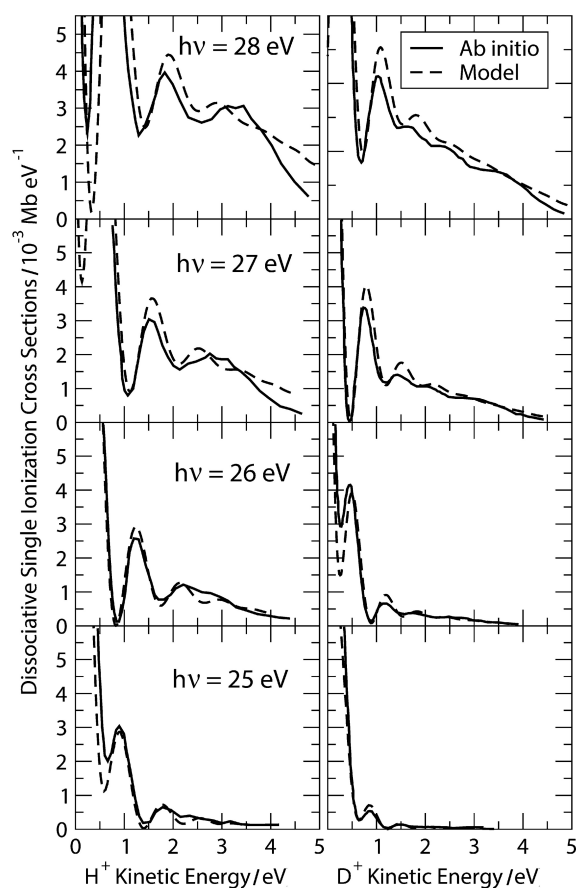


**Figure 2.** Dissociative ionization cross sections. Left panels:  $H_2$ . Right panels:  $D_2$ . Dashed line: model. Solid line: ab initio calculations from ref. [48].

parallel to the molecular axis. Due to the selection rules, this implies that only the final states with  $1^1\Sigma_u^+$  symmetry are populated. The potential energy curve  $V_p(R)$  for the first ionization threshold  $1s \sigma_g$  has been calculated analytically and that of the  $1Q_1 1^1\Sigma_u^+$  DES has been taken from our ab initio calculations (both plotted in Figure 1). For the vibrational ground state of  $H_2$  (and  $D_2$ ), we have solved the 1D Schrödinger equation using the accurate electronic energies obtained by Wolnievicz.<sup>[51,52]</sup>

Notice that the values of  $\delta_c$ ,  $d_Q$ , and  $d_p$  should be the same for both isotopes because they only depend on the electronic structure. This requirement has been imposed for the fit shown in Figure 2. Moreover, for simplicity we have also imposed  $\delta_c$ ,  $d_Q$ , and  $d_p$  to be independent of photon and electron energy, assuming negligible variation in the relatively narrow photon energy range we are fitting, from 25 to 28 eV. For the results shown in Figure 2, we find  $\delta_c \approx 4\pi/3$  and  $d_Q/d_p \approx 0.15$  (the remaining global scale depends on whether we compare with a cross section or a probability obtained from a short pulse calculation). This compares well with the ratio obtained by averaging the actual value over the FC region and contributing electron energies, which is  $|d_Q/d_p| \approx 0.09$ . The agreement of the model with the ab initio calculations of ref. [48] is remarkable, especially because all the  $\varepsilon$  dependencies have been neglected for the amplitudes. From this comparison, we can essentially conclude that the strong oscillations appearing in

the low proton (deuteron) kinetic energy regions are due to the interference of the two classical paths followed by the nuclei. This demonstrates unambiguously that the origin of the interference structures in the nuclear kinetic energy distribution is different from that of Fano interferences since the latter are not included in the model. They are instead caused purely by the phase acquired in nuclear motion. Although we focus on dissociative ionization here, we note that the model also reproduces qualitatively the oscillations seen in nondissociative ionization as a function of photoelectron energy, and their change with nuclear mass as predicted in ref. [53], indicating that these oscillations are caused by nuclear effects as well, and are not related to Fano lineshapes.

Naturally, the question arises whether the model could be used to extract  $\Gamma(R)$ , given the photoionization cross sections. Note that  $\Gamma(R)$  contains the actual electron–electron correlation information among direct and autoionization paths. The extraction of the width from experimentally measured energy-differential cross sections was already attempted,<sup>[33,54]</sup> although those works lacked the description of the interference term in Equation (3) and directly fitted Equation (1), which is partly the origin of the discrepancies found for their extracted widths in comparison with the most accurate values given in ref. [47]. Here, we should also point out that the results in ref. [48] were obtained by considering only one autoionization state (the lowest in the  $Q_1$  series of  $1\Sigma_u^+$  symmetry), although the coupling with the other DESs of the series was included. This choice was appropriate since the  $1Q_1 1\Sigma_u^+$  state is the main state contributing in the photon energy region  $\leq 28$  eV. However, other DESs also contribute to the actual photoionization process, so that the agreement with the model is expected to be worse for a more complete calculation or an experiment, making extraction of  $\Gamma(R)$  significantly more challenging.

Thus using the method of ref. [23], we have performed ab initio calculations in which all the DESs of the  $Q_1$  series are included, extracting the cross sections as described in ref. [55]. The results for the latter calculations, as well as for the model using the calculated and the fitted  $\Gamma(R)$  are plotted in Figure 3. It shows the photoionization cross sections as a function of photon energy and energy sharing among nuclei and electrons (the ratio between the nuclear kinetic energy and the total available energy  $E_T$ ). Figure 3a corresponds to the ab initio calculation including the complete  $Q_1$  series. The newly computed cross sections are extremely similar to those in Figure 3b where only the first DES of the series is included, that is, results as in ref. [48]. The only appreciable difference appears for photon energies above 28 eV and for energy sharing above 20–30%, where, as expected, we find slightly larger ionization yields due to the contribution from higher DESs in the  $Q_1 1\Sigma_u^+$  series. The two lowest panels in Figure 3 correspond to the cross sections obtained with the semiclassical model using the calculated width (Figure 3c) and, more interestingly, when fitting the  $\Gamma(R)$  function (Figure 3d). For this last case,  $\delta_c$ ,  $c_p$  and  $c_Q$  are left as free energy-independent parameters and we find the function  $\Gamma(R)$  that leads to the best agreement of Equation (3) with the ab initio calculated cross sections including a single DES (i.e. Figure 3b).

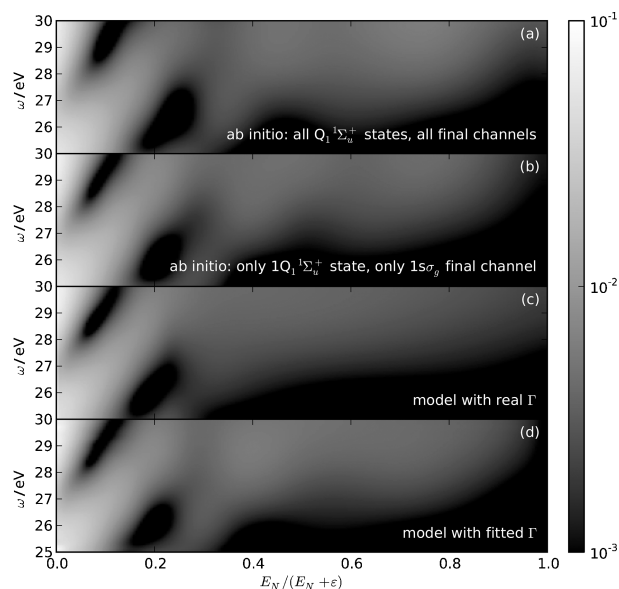


**Figure 3.**  $H_2$  dissociative ionization probability as a function of photon energy (y-axis) and energy sharing (x-axis, ratio of nuclear and total kinetic energy available). (a) Full ab initio calculations. (b)  $1s \sigma_g$  final channel from ab initio calculations including only the first DES in the  $Q_1 1\Sigma_u^+$  series. (c) Simple model in Equation (3) using the calculated values for  $\Gamma(R)$  given in ref. [48]. (d) Simple model in Equation (3) with  $\Gamma(R)$  obtained by fitting to (b).

The corresponding fitted  $\Gamma(R)$  is shown in Figure 4 in dashed thick lines and compared with the calculated width (full thick line). The fitted values start at around  $R = 1.42$  a.u. since this is the smallest internuclear distance that is reached by the largest photon energy,  $\omega = 30$  eV, included for the fit. The agreement is quite reasonable up to an internuclear distance of 3 a.u., that is, well beyond the Franck–Condon region. At larger  $R$  values, the width is overestimated. This could be expected from the assumptions that are implicit in the semiclassical model: 1) it is assumed that the autoionization events eject electrons with a well-defined energy at a given internuclear distance, whereas in the quantum treatment the electron ejection occurs in an interval of energies with a bandwidth of  $\Gamma(R)$  around the energy of the DES,  $V_Q(R)$ ; and 2) the amplitudes are

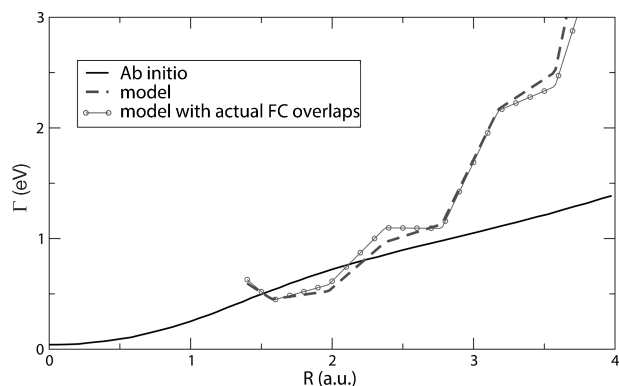


**Figure 4.** Autoionization decay width  $\Gamma(R)$  (in eV) obtained by fitting Equation (3) to ab initio  $H_2$  data. Dashed line: fit using the reflection approximation. Solid line with circles: fit using the actual FC overlaps.

approximated by using the reflection approximation and neglecting the energy and  $R$  dependencies of the transition elements, whose error is expected to accumulate in the integrals performed in increasingly larger intervals of internuclear distances. In order to further check the validity of the fit, in Figure 4, we have also included the values of  $\Gamma(R)$  obtained from an additional fit in which the actual FC overlaps between the vibrational ground state and the final resonant and non-resonant states are included. As expected, the extracted widths do not differ from those resulting from the previous fit, because the steep shape of the potential energy curves in the region of maximum vibrational overlap validates the reflection approximation assumed in the first fit (Supporting Information).

The appropriateness of the model in describing energy-differential cross sections, in particular, the interferences resulting from different dissociation pathways, and in providing a reasonable value of  $\Gamma(R)$  up to relatively large values of  $R$ , raises the challenge of its applicability in the time domain in order to understand the outcome of pump-probe experiments aimed at getting insight in the autoionization dynamics. Such experiments have already been performed on atoms<sup>[15]</sup> and on hydrogenic molecules.<sup>[28]</sup> The ultimate goal is to trace molecular autoionization in time. In the following we show the temporal build-up of the interference by means of both time-dependent ab initio calculations and the simple model, where we now introduce the time dependence of the nuclear position.

### 3. Time-Resolved Build-Up of Molecular Autoionization Features

For a time-resolved image of the decay into the continuum obtained through ab initio calculations we take advantage of our time-dependent Feshbach-like methodology (for details, see refs. [23, 55, 56]). The partition of the Hamiltonian in two subspaces allows a direct projection into the  $P$  subspace of the field-free propagated wavepacket at different times. We use a low-intensity ( $10^{12} \text{ W cm}^{-2}$ ) 500 as pulse centered at 28 eV and extract the apparent cross sections (i.e. those resulting from the probabilities at a given time, despite the fact that cross sections are only well-defined in the asymptotic limit, see ref. [55] for details) in the range from 25–28 eV, for which the energy components of the Fourier-transformed pulse are appreciably non-zero. We then take snapshots of the apparent cross sections every 500 as after the end of the pulse. Their time evolution is plotted in the left-side panels of Figure 5 for four different photon energies. The thin full line in each panel corresponds to the long-time limit (i.e. the actual cross section). For completeness, we have also included the time-independent calculations from ref. [48] (dashed lines). We here compare to the time-dependent calculations where only the lowest DES is included, as in Figure 3b and ref. [48]. Right at the end of the pulse ( $t = T = 0.5$  fs), only direct photoionization is observable. 500 as later ( $t = 1.0$  fs), autoionization leads to ions with energies up to 2.5 eV and interferes with the direct ionization channel. As time passes, larger proton kinetic energies are observed, and the interference builds up. At  $t = 3.0$  fs,

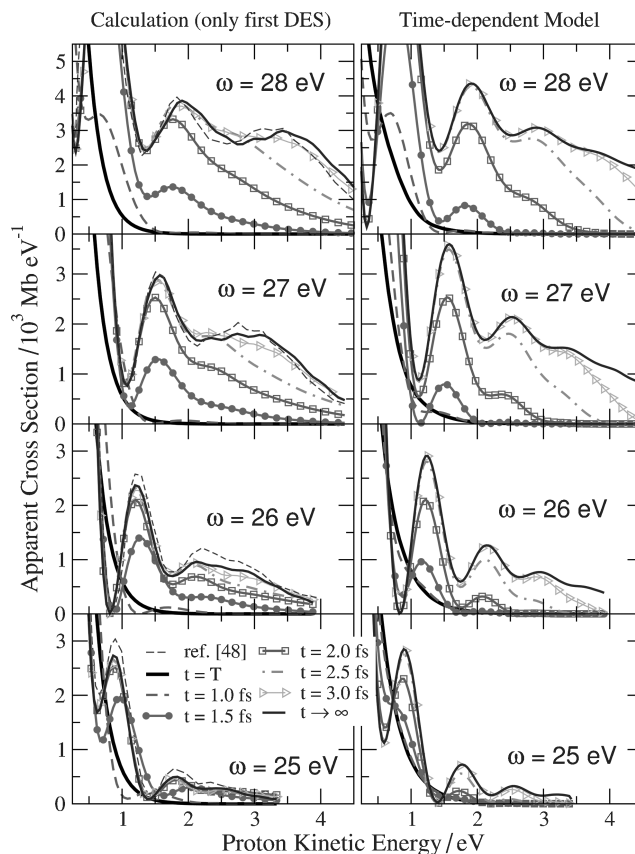


**Figure 5.** Field-free evolution of  $\text{H}_2$  dissociative ionization apparent cross sections at different times after the end of a  $T = 500$  as pulse. Left panels: ab initio calculations including the first  $^1\Sigma_u^+$  DES. Right panels: time-dependent model. Each row correspond to a given photon energy. Solid thin lines correspond to the probabilities in the long-time limit. Dashed thin lines are time-independent calculations taken from ref. [48].

that is, 2.5 fs after the end of the 500 as pulse, autoionization has practically finished and the apparent cross sections have reached their asymptotic form. However, the time evolution of the observed structures remains to be explained. Is this evolution determined by electron correlation (and thus comparable to structures in atomic systems) or by nuclear motion (and thus of purely molecular origin)?

In order to properly answer this question, we investigate the nuclear dynamics in more detail. While the direct contribution “instantaneously” populates the nuclear continuum, the contribution from the DESs depends on time. The laser pulse creates a nuclear wave packet in the DESs, which then slides down the  $V_Q(R)$  curve, accelerating in the process. Snapshots of this wave packet as extracted from the full ab initio calculation are shown in Figure 6. As the wave packet passes over a given internuclear distance  $R$ , it ejects electrons at the associated energy  $\varepsilon = V_Q(R) - V_P(R)$ , which also determines the asymptotic nuclear energy  $E_N = E_T - \varepsilon$ . We include this behavior in the semi-classical expression defined in Equation (3), to give Equation (8):

$$P(\varepsilon, E_N, t) = |c_P e^{-i\theta_P - i\delta_\varepsilon} + g(t, \varepsilon) a_Q e^{-i\theta_Q}|^2 \quad (8)$$

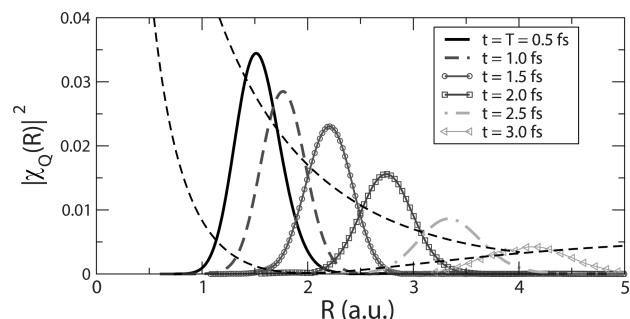


**Figure 6.** Field-free propagation of the vibrational wave packet associated to the  $1Q_1, 1\Sigma_v^+$  state, launched from the ground state by a 500 as pulse centered at 28 eV.

where  $g(t, \varepsilon)$  is a time-dependent filter representing the accumulated amplitude of the nuclear wavepacket  $\chi_Q$  passing over the internuclear distance  $R^d$  where electrons of energy  $\varepsilon$  are ejected,  $g(t, \varepsilon) = \int_{-\infty}^t dt |\chi_Q(R^d(\varepsilon), t)|$ . Note that the nuclear phase is fixed and given by  $\theta_Q$ , and the filter only affects the amplitude of the DES contribution. For simplicity, we furthermore neglect dispersion of the nuclear wave packet and approximate it as a Gaussian with a constant spatial width  $\sigma_R \approx 0.25$  a.u. (corresponding to the average width from a vertical transition with a 500 as pulse). To avoid requiring quantum wave packet propagation, we approximate the motion of the center of the Gaussian by classical mechanics,  $\mu \ddot{R} = -dV_Q/dR$ , with initial conditions  $R(T/2) = R_Q^0$  and  $\dot{R}(T/2) = 0$  at the peak  $T/2 = 250$  as of the pulse. This gives the classical trajectory for  $R(t)$  which defines the time  $t_d$  at which the wave packet passes the point of decay,  $R^d = R(t_d)$ . By additionally approximating the velocity as locally constant,  $\dot{R}(t) \approx \dot{R}(t_d)$ , the integral for  $g(t, \varepsilon)$  can be analytically evaluated,  $g(t, \varepsilon) = 0.5 \operatorname{erfc}[-(t - t_d)/\sigma_t]$ , with  $\sigma_t = \sigma_R / \dot{R}(t_d)$ .

The time-dependent probabilities obtained with this simple model appear in the right-side panels of Figure 5. Again, the agreement with the ab initio calculations is excellent, except at high proton energies. Apart from the interference with the  $P$  background, the observed temporal dependence is simply that of the vibrational wavepacket motion in the metastable  $Q$  electronic state. The snapshots at different times thus reveal the expected profile of electron ejection from the moving nuclear wave packet. The answer to the question posed above is thus that the nuclear motion indeed determines the time at which the contribution at a given proton kinetic energy appears in the spectrum. Electron correlation only governs the local decay rate  $\Gamma(R)$ , which dictates how much autoionization occurs.

It should be remarked that our benchmark system,  $H_2$ , is particular in the sense that both nuclear and autoionization dynamics are relatively fast and occur over similar time intervals (a few fs). In most cases, the nuclei have enough time to move before autoionization occurs. Thus, in an eventual generalization of our semiclassical approach to larger molecules, one should first analyze if similar time scales apply. For example, for much heavier targets with significantly slower nuclear dynamics, autoionization may occur well before the nuclei move appreciably and, consequently, the energy dependence of the

interference between the electronic continuum and the resonance [described by  $\Delta$  in Eq. (2)] should not be neglected. Also, for such heavy targets, the FC region could be so narrow that for all practical purposes the absorption of a photon would be described by a vertical transition. Under these circumstances, one would expect photoelectron spectra similar to those observed in atoms, with peaks exhibiting standard Fano line shapes.

## 4. Conclusions

We have presented a simple model to describe the features appearing in the energy-differential cross sections for dissociative molecular autoionization. To enable an appropriate comparison, we use hydrogenic molecules as benchmark systems, for which accurate experimental and theoretical photoionization cross sections in the region where doubly excited states are populated are available. The semiclassical model proposed here is based on well-established models for Penning ionization,<sup>[33,44–46]</sup> while also accounting for the presence of direct ionization, which interferes coherently with autoionization. We show that this interference is responsible for the pronounced structures observed at low nuclear kinetic energies and is well-described by the phase accumulated along two classical paths followed by the nuclei. The observed interferences are thus found to be mainly governed by nuclear effects and fundamentally different from a Fano profile, the structure observed in atomic systems.

The temporal build-up of these interferences has also been studied. The time evolution of the energy-differential apparent cross sections is found to be accurately represented within our semiclassical approach as well, as demonstrated by its excellent agreement with the solution of the time-dependent Schrödinger equation. This evolution is again shown to be dominated by nuclear dynamics. The electronic decay rate  $\Gamma$  determines the amplitude of the contribution at a given nuclear kinetic energy, but the timing is determined by how long the nuclear wavepacket takes to accelerate to the given energy as it slides down the  $V_Q(R)$  potential curve.

## Acknowledgements

We thank Mare Nostrum BSC and CCC-UAM for allocation of computer time. Work supported by the Advanced Grant of the European Research Council XCHEM 290853, the European grants MC-ITN CORINF and MC-RG ATTOTREND, the European COST Action CM0702, the MICINN project Nos. FIS2010-15127, ACI2008-0777 and CSD 2007-00010 (Spain), and the ERA-Chemistry project PIM2010EEC-00751. A.P. acknowledges a Juan de la Cierva Contract grant from MICINN. J.F. thanks the NSF for support through a grant to ITAMP. J.L.S.-V. acknowledges financial support from Vicerrectoría de Investigación (contract number E01538 and Estrategia de Sostenibilidad 2013-2014) at Universidad de Antioquia.

**Keywords:** ab initio calculations • autoionization • electron-electron correlation • molecular hydrogen • photochemistry

- [1] A. H. Zewail, *J. Phys. Chem. A* **2000**, *104*, 5660.
- [2] A. Stolow, A. E. Bragg, D. M. Neumark, *Chem. Rev.* **2004**, *104*, 1719.
- [3] J. Seres, E. Seres, A. J. Verhoef, G. Tempea, C. Strelci, P. Wobrauschek, V. Yakovlev, A. Scrinzi, C. Spielmann, F. Krausz, *Nature* **2005**, *433*, 596.
- [4] A. H. Zewail, *Ann. Rev. Phys. Chem.* **2006**, *57*, 65.
- [5] M. Drescher, M. Hentschel, R. Kienberger, G. Tempea, C. Spielmann, G. A. Reider, P. B. Corkum, F. Krausz, *Science* **2001**, *291*, 1923.
- [6] M. Hentschel, R. Kienberger, C. Spielmann, G. A. Reider, N. Milosevic, T. Brabec, P. Corkum, U. Heinzmann, M. Drescher, F. Krausz, *Nature* **2001**, *414*, 509.
- [7] P. Salières, M. Lewenstein, *Meas. Sci. Technol.* **2001**, *12*, 1818.
- [8] G. Sansone, E. Benedetti, F. Calegari, C. Vozzi, L. Avaldi, R. Flammini, L. Poletto, P. Villoresi, C. Altucci, R. Velotta, et al., *Science* **2006**, *314*, 443.
- [9] J. Ullrich, R. Moshhammer, A. Dorn, R. Dörner, L. P. H. Schmidt, H. Schmidt-Böcking, *Rep. Prog. Phys.* **2003**, *66*, 1463.
- [10] C. Bostedt, H. N. Chapman, J. T. Costello, J. R. C. López-Urrutia, S. Düsterer, S. W. Epp, J. Feldhaus, A. Föhlisch, M. Meyer, T. Möller, et al., *Nucl. Instrum. Methods Phys. Res. Sect. A* **2009**, *601*, 108.
- [11] J. Mauritsson, T. Remetter, M. Swoboda, K. Klünder, A. L'Huillier, K. J. Schafer, O. Ghafur, F. Kelkensberg, W. Siu, P. Johnsson, et al., *Phys. Rev. Lett.* **2010**, *105*, 053001.
- [12] E. Goulielmakis, Z.-H. Loh, A. Wirth, R. Santra, N. Rohringer, V. S. Yakovlev, S. Zherebtsov, T. Pfeifer, A. M. Azzeer, M. F. Kling, et al., *Nature* **2010**, *466*, 739.
- [13] P. M. Paul, E. S. Toma, P. Breger, G. Mullot, F. Augé, P. Balcou, H. G. Muller, P. Agostini, *Science* **2001**, *292*, 1689.
- [14] M. Drescher, M. Hentschel, R. Kienberger, M. Uiberacker, V. Yakovlev, A. Scrinzi, T. Westerwalbesloh, U. Kleineberg, U. Heinzmann, F. Krausz, *Nature* **2002**, *419*, 803.
- [15] S. Gilbertson, M. Chini, X. Feng, S. Khan, Y. Wu, Z. Chang, *Phys. Rev. Lett.* **2010**, *105*, 263003.
- [16] U. Fano, *Phys. Rev.* **1961**, *124*, 1866.
- [17] M. Wickenhauser, J. Burgdörfer, F. Krausz, M. Drescher, *Phys. Rev. Lett.* **2005**, *94*, 023002.
- [18] T. Mercouris, Y. Komninos, C. A. Nicolaides, *Phys. Rev. A* **2007**, *75*, 013407.
- [19] W.-C. Chu, C. D. Lin, *Phys. Rev. A* **2010**, *82*, 053415.
- [20] W.-C. Chu, C. D. Lin, *Phys. Rev. A* **2012**, *85*, 013409.
- [21] A. Palacios, H. Bachau, F. Martín, *Phys. Rev. Lett.* **2006**, *96*, 143001.
- [22] A. Palacios, H. Bachau, F. Martín, *Phys. Rev. A* **2006**, *74*, 031402.
- [23] J. L. Sanz-Vicario, H. Bachau, F. Martín, *Phys. Rev. A* **2006**, *73*, 033410.
- [24] A. Palacios, H. Bachau, F. Martín, *Phys. Rev. A* **2007**, *75*, 013408.
- [25] J. D. Bozek, J. E. Furst, T. J. Gay, H. Gould, A. L. D. Kilcoyne, J. R. Machacek, F. Martín, K. W. McLaughlin, J. L. Sanz-Vicario, *J. Phys. B* **2006**, *39*, 4871.
- [26] J. F. Pérez-Torres, F. Morales, J. L. Sanz-Vicario, F. Martín, *Phys. Rev. A* **2009**, *80*, 011402.
- [27] F. Morales, J. F. Pérez-Torres, J. L. Sanz-Vicario, F. Martín, *Chem. Phys.* **2009**, *366*, 58.
- [28] G. Sansone, F. Kelkensberg, J. F. Pérez-Torres, F. Morales, M. F. Kling, W. Siu, O. Ghafur, P. Johnsson, M. Swoboda, E. Benedetti, et al., *Nature* **2010**, *465*, 763.
- [29] D. Dowek, J. F. Pérez-Torres, Y. J. Picard, P. Billaud, C. Elkharrat, J. C. Houver, J. L. Sanz-Vicario, F. Martín, *Phys. Rev. Lett.* **2010**, *104*, 233003.
- [30] J. F. Pérez-Torres, J. L. Sanz-Vicario, H. Bachau, F. Martín, *J. Phys. B* **2010**, *43*, 015204.
- [31] F. Kelkensberg, W. Siu, J. F. Pérez-Torres, F. Morales, G. Gademann, A. Rouzée, P. Johnsson, M. Lucchini, F. Calegari, J. L. Sanz-Vicario, et al., *Phys. Rev. Lett.* **2011**, *107*, 043002.
- [32] W. H. Miller, *J. Chem. Phys.* **2012**, *136*, 210901.
- [33] C. J. Latimer, A. D. Irvine, M. A. McDonald, O. G. Savage, *J. Phys. B* **1992**, *25*, L211.
- [34] C. J. Latimer, K. F. Dunn, N. Kouchi, M. A. McDonald, V. Srigengan, J. Geddes, *J. Phys. B* **1993**, *26*, L595.
- [35] K. Ito, R. I. Hall, M. Ukai, *J. Chem. Phys.* **1996**, *104*, 8449.
- [36] M. Leventhal, R. T. Robiscoe, K. R. Lea, *Phys. Rev.* **1967**, *158*, 49.
- [37] J. Geddes, K. F. Dunn, N. Kouchi, M. A. McDonald, V. Srigengan, C. J. Latimer, *J. Phys. B* **1994**, *27*, 2961.
- [38] F. Martín, *J. Phys. B* **1999**, *32*, R197.
- [39] A. Lafosse, M. Lebeck, J. C. Brenot, P. M. Guyon, L. Spielberger, O. Jagutzki, J. C. Houver, D. Dowek, *J. Phys. B* **2003**, *36*, 4683.
- [40] F. Martín, J. Fernández, T. Havermeier, L. Foucar, T. Weber, K. Kreid, M. Schöffler, L. Schmidt, T. Jahnke, O. Jagutzki, et al., *Science* **2007**, *315*, 629.
- [41] T. J. Reddish, A. Padmanabhan, M. A. MacDonald, L. Zuin, J. Fernández, A. Palacios, F. Martín, *Phys. Rev. Lett.* **2012**, *108*, 023004.
- [42] P. Billaud, M. Géléoc, Y. J. Picard, K. Veyrinas, J. F. Hergott, S. Marggi Poullain, P. Breger, T. Ruchon, M. Rouillay, F. Delmotte, et al., *J. Phys. B* **2012**, *45*, 194013.
- [43] I. Sánchez, F. Martín, *J. Phys. B* **1997**, *30*, 679.
- [44] W. H. Miller, *J. Chem. Phys.* **1970**, *52*, 3563.
- [45] J. C. Browne, A. Dalgarno, *J. Phys. B* **1969**, *2*, 885.
- [46] A. U. Hazi, *J. Chem. Phys.* **1974**, *60*, 4358.
- [47] I. Sánchez, F. Martín, *J. Chem. Phys.* **1997**, *106*, 7720.
- [48] I. Sánchez, F. Martín, *Phys. Rev. A* **1998**, *57*, 1006.
- [49] I. Sánchez, F. Martín, *J. Chem. Phys.* **1999**, *110*, 6702.
- [50] H. Feshbach, *Ann. Phys.* **1962**, *287*, 19.
- [51] L. Wolniewicz, K. Dressler, *J. Chem. Phys.* **1985**, *82*, 3292.
- [52] L. Wolniewicz, *J. Chem. Phys.* **1993**, *99*, 1851.
- [53] I. Sánchez, F. Martín, *J. Chem. Phys.* **1997**, *107*, 8391.
- [54] K. Kirby, T. Uzer, A. C. Allison, A. Dalgarno, *J. Chem. Phys.* **1981**, *75*, 2820.
- [55] A. González-Castrillo, A. Palacios, F. Catoire, H. Bachau, F. Martín, *J. Phys. Chem. A* **2012**, *116*, 2704.
- [56] J. L. Sanz-Vicario, A. Palacios, J. C. Cardona, H. Bachau, F. Martín, *J. Electron Spectrosc. Relat. Phenom.* **2007**, *161*, 182.

Received: November 24, 2012

Published online on March 14, 2013